BJES Basrah Journal for Engineering Sciences

Basrah Journal for Engineering Sciences, Vol. 23, No. 2, (2023), 34-44

Original Article

Journal homepage: www.bjes.edu.iq
ISSN (Online): 23118385, ISSN (Print): 18146120

OPEN ACCESS

Automatic Feature Extraction Based on Envelope Analysis and its Application in Rolling-Element Bearing Fault Detection

Haider Suhail Najim [1, *], Jaafar Khalaf Ali [2]

Department of Mechanical Engineering, College of Engineering, University of Basrah, Basrah, Iraq
E-mail addresses: pgs2404@uobasrah.edu.iq , Jaafar.ali@uobasrah.edu.iq
Received: 7 December 2022; Accepted: 11 January 2023; Published: 30 December 2023

Abstract

Bearing fault diagnosis is essential for the maintenance, durability, and reliability of rotating machines. It can minimize economic losses by removing unplanned downtime in the industry due to the failure of rotary machines. In bearing fault detection, developing fault features extraction techniques that can successfully applicable for various fault severity and different operating conditions is still a critical issue. In the current work, the feature extraction technique is a combination between pre-processing algorithms and envelope analysis method. In the pre-processing stage, the autoregressive (AR) model is used to filter the original signal and remove the deterministic vibration sources, as well as maintain the signal representing the condition of the bearing without contaminating noises. Then, the most suitable frequency band is selected based on the spectral kurtosis (SK) analysis. This band contains the signature frequencies of the roller bearing. After that, envelope analysis is employed for detecting faults at different severity. Finally, the features represented the peaks at fundamental fault frequencies are automatically selected from the envelope spectrum. By analyzing all diagnoses results, it is found that the presented method effectively extracts the features at calculated resonance bearing frequencies and proves the significance of the enhancements in a pre-filtering stage in the overall detection performance. Also, it can benefit from these features in the fault classification fields at different speeds because it is independent of speed variation.

Keywords: Envelope Analysis, Frequency Features, Spectral Kurtosis, Fundamental Fault Frequencies

http://doi.org/10.33971/bjes.23.2.5

1. Introduction

Rolling element bearings are essential components in every rotating machinery, failure of roller bearings may lead to catastrophic breakdown and expensive downtime. Therefore, bearing defect detection attracts a lot of attention and has been the topic of extensive studies [1]. Bearing condition monitoring and defect diagnosis is highly demanded in modern machinery maintenance techniques. Due to the multiple vibration sources in rotating machinery, the vibration signals are contaminated by noise and random patterns; as a result, it is difficult to capture the fault conditions, especially in the early stage of the defect [2]. The envelope analysis method is robust for roller-bearing defect diagnoses. When a defect initiation, such as a small pit or crack in an operating surface of the roller bearing, impacts another contact bearing part, a strike is produced that causes resonances phenomenon in rotating machine parts. As the roller bearings works, strikes will happen periodically with an associated roller bearing fundamental frequencies, which are specially obtained by the placement of the defect on one of the rolling parts, inner race, and outer race [3]. In the traditional envelope analysis, the band-pass frequency filter concentrated at a resonance frequency of roller bearing with a bandwidth equal to the tin time of inner pass frequency is employed to the original signal. Most of the surrounding vibration signal from other rotating machine components is removed, resulting in the isolation of a resonance band. In this way, the faults vibration information from the roller bearing can be recognized, even in complicated machines such as a compressor. After filtering, the signal is demodulated using the Hilbert transform technique to produce its frequency spectrum. Then, it is possible to detect the roller bearing defect by the appearance of a final spectral diagram associated with a fault in the inner race, outer race, or one or more of the rolling elements. Furthermore, the selection of band frequency has a direct significant on the performance of envelope analysis. The selection of band frequency directly impacts the performance of envelope analysis [4]. The proper frequency band is still a challenging issue. The easiest approach is to set a wide band such as (e.g., 1–40 kHz), which includes resonance frequencies of bearing. However, the large band also contains dominant vibration signals from other machine parts such as gearbox, motors, etc. In addition, the wide frequency band, which includes high noise levels, hinders the envelope analysis's effectiveness in roller-bearing defect detection [5].

Bechhoefer et al. [6] developed a method to obtain the best frequency bandwidth window for the envelope analysis method. In their approach, envelope kurtosis and spectral kurtosis are tools for getting the best frequency and bandwidth window. Meanwhile, it established a measure of effectiveness, which is a correlation between the fault of energy with total defect length. This parameter evaluated the ability of spectral

kurtosis/envelope kurtosis to predict the best envelope detection window.

Amini et al. [7] applied the acoustic emission envelope analysis for detecting faults in train axle bearing. For comparison, two types of datasets were recorded one actual from freight wagons with artificially defected axle bearings and the other from a customized test rig in a laboratory. They concluded that the envelope analysis method is feasible and effective for the detection of faults in train axle bearing in real-world conditions.

Xu et al. [8] investigated how to obtain the best resonance frequency band by using the enhanced Automatic band selection algorithm. Their method, firstly, applied time synchronous averaging and high-pass filtering to eliminate dominant speed-dependent (synchronous and nonsynchronous) spectral contents of the original vibration signal. Then, employed the wavelet packet transform and RMS to obtain the energy distribution of the residual vibration signal. Finally, selected the band with the highest energy contents for envelope analysis. Their results indicated that the proposed method is more useful than the present band selection technique and requires no advanced sensor technology.

Jia et al. [9] developed a two-stage technique for the identification of weak signals in roller bearing. Their method is based on a combination of cyclic Wiener filter and improved enhanced envelope spectrum. Firstly, processed the raw vibration signal by cyclic Wiener filter exploiting the spectral coherence approach and the noises are filtered out. Subsequently, obtained the enhanced envelope based on the sensitive frequency band. The innovation of the suggested technique is to fully excavate the advantages of cyclic Wiener filter and enhanced envelope simultaneously.

As a result of the mentioned research above, the traditional envelope analysis becomes very effective in severe fault cases and clearly distinguishes the fault characteristics. In many cases, the effectiveness of envelope analysis in extracting accurate fault information becomes unreliable when dealing with weak fault signals, particularly in the early stages of fault growth. Hence, to overcome this limitation it is important to modify the envelope analysis procedure. This work has two goals. First, improve the envelope detection process in obtaining the best frequency band and extracting automatic fault features. The second goal is employing the frequency fault features extracted from envelope analysis in machine learning techniques.

The remainder of this paper is organized as follows: The methodology of the suggested faults bearing diagnosis approach and the main process are introduced in Section II. Fault diagnosis experiments for rolling bearing are presented in Section III. The actual experimental evaluation and results analysis of the suggested method are described in Section IV. Finally, the conclusions are discussed in Section V.

2. Methodology

This section highlights the frequency feature extraction and the main process of the fault-bearing model. The proposed automatic features extraction workflow for detection rolling bearing faults is shown in Fig. 1. The first stage included recording data from roller bearing with different levels of severe fault, various fault locations and multiple motor speeds. then, applying some important pre-processing enhancements methods that can be summarized as segmentation of every long data into equal time duration, removing the deterministic component from vibration data, and selecting the best frequency band which contains the most faults information. Finally, the modified envelope analysis is employed for extraction features at resonance bearing frequencies automatically. The main advantage of the suggested feature extracted technique is independent of speed and can be utilized from this in fault diagnosis and classification at different speeds and various of roller bearing types.

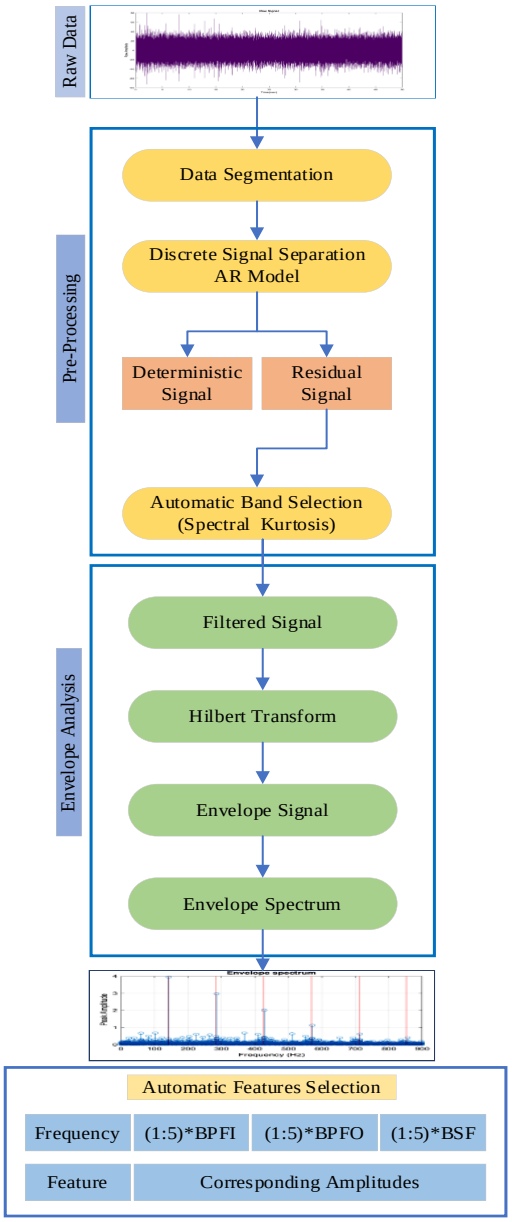

Fig .1 Flow chart of proposed fault diagnosis model

2.1. *Fundamental Fault Frequencies*

A typical rolling element bearing has four main parts: the inner race (IR), the outer race (OR), the rolling elements (RE), and the cage(C). At the constant shaft speed of rotary machines, when a roller bearing has cracks or defects in any of

these parts, periodic vibration signals are generated, which produce a signal like the one in Fig.2. There are four basic fault frequencies: BPFI (ball pass frequency, inner race), BPFO (ball pass frequency, outer race), BSF (ball spin frequency), and FTF (fundamental train frequency). According to [10], the fault frequencies can be mathematically represented as follows.

$$BPFI = \frac{n\,f_s}{2}\,(1 + \frac{d}{D}cos\,\alpha) \quad (1)$$

$$BPFO = \frac{n\,f_s}{2}\,(1 - \frac{d}{D}cos\,\alpha) \quad (2)$$

$$BSF = \frac{D\,f_s}{2d}\,(1 - (\frac{d}{D}cos\,\alpha)^2) \quad (3)$$

$$FTF = \frac{f_s}{2}\,(1 - \frac{d}{D}cos\,\alpha) \quad (4)$$

where *fs* is the shaft speed, *n* is the number of rolling elements, and α is the contact angle, *d and D* represent ball diameter and pitch diameter, respectively. Theoretically, if the defect appears on any of the bearing components, a vibration signal is generated whenever the roller elements impact the defects component. The signal strength is directly affected by defects severity. The fundamental frequencies are beneficial for recognizing faults on the outer race, inner race, and the rolling element. These fault frequencies can appear and be captured via envelope analysis.

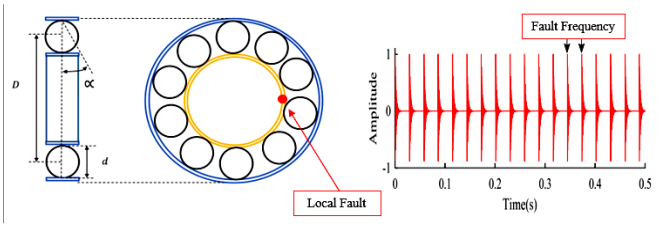

Fig.2 Bearing geometry and strike signal [11].

2.2 Pre-Processing Algorithms

2.2.1. Discrete Signal Separation

In The second step, remove the discrete (deterministic) signal generated from other vibration sources, such as shafts. The separation can be achieved by the autoregressive (AR) model and can be obtained by calculating the present time data value via the weighted sum of previous time values. As demonstrated in Fig.3, the discrete component of the autoregressive model is then subtracted from the raw signal to produce the residual signal. Also, the AR model can be constructed by using the following equations [12].

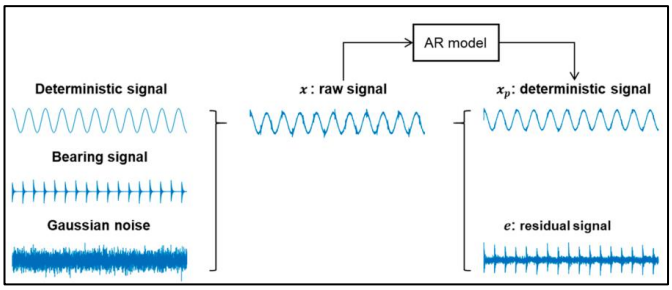

Fig.3 Process flow for obtaining the residual signals [13]

$$x_p(n) = -\sum_{k=1}^{p} a(k) * x(n-k) \quad (5)$$

$$in\ matrix\ form\ \ x_p = -x_a \quad (6)$$

Where x(n) is the raw signal, x_p is deterministic signal at nth time step, a(k) weighting coefficients and can be calculated by solving Yule-Walker equation and x(n-k) is n-k^{th} data. The order p directly influences the prediction accuracy, it should be calculated to ensure the residual vibration signal represents the defect as best as possible. There are several methods for obtaining the order p in this paper from the following equation.

$$order\ P = \frac{sample\ rate\ \ frequncy}{maximum\ funamental\ bearing\ frequncy} \quad (7)$$

2.2.2. *Automatic Band Selection*

The band selection is a crucial point in the overall envelope detection performance. For this purpose, in the third stage of pre-processing of vibration signal, a frequency band containing the roller bearing resonance frequencies capturing from residual signal. In addition, the modified automatic selection is based on the spectral kurtosis (SK) approach, which is the kurtosis in the time-frequency schema at each frequency line. When the defect is present, the SK values rise around the area of resonance frequencies of bearing and automatically select the maximum value with narrow bandwidth onto which the residual signal is filtered based on it. The short-time Fourier transform (STFT) functions is employed to define SK such as in the following equations [14].

$$k(f) = \frac{\langle |s(t,f|^4 \rangle}{\langle |s(t,f)^2 \rangle^2} - 2 \quad (8)$$

Where $\langle . \rangle$is the time-averaging operator, and *s (t, f)* is the STFT of the residual signal. The STFT represents a local Fourier transform for a specific time window. This paper uses the Hann window, one of several window functions, with length L and calculated based on the following equation. Also, can explain the frequency band selection procedure in Fig 4.

$$w(l) = 0.5\left(1 - cos\left(2\pi\frac{l}{L-1}\right)\right), 0 \le l \le L-1 \quad (9)$$

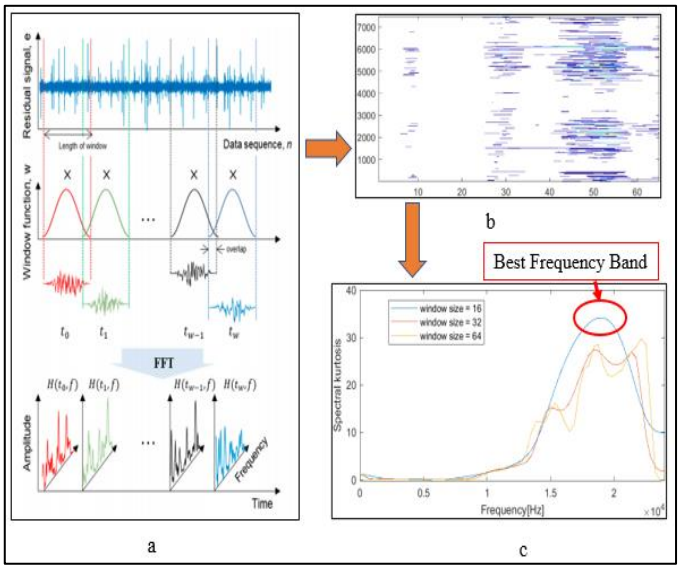

Fig.4 Automatic frequency band selection steps (a) Concept of STFT (b) Results of STFT (c) Result of SK

2.2. Envelope Spectrum Analysis

The aim of envelope analysis is to isolate the bearing signal from the raw signal interfaces with other noisy sources and make the fault information more distinguished. The essential steps of envelope detection and frequency feature selection can be summarized as applying bandpass filtering to the residual signal, constructing the envelope signal and the envelope spectrum calculation. In the first step, using a bandpass filter to the remaining signals within the band only. After that, the envelope of the bearing vibration signal can be determined by using the Hilbert transform. This technique is employed to obtain a complex real part from the original signal where the imaginary part is a phase-shifted copy of the real component, which can be calculated using the following equations [15].

$$H\left[s(t)\right] = s(t) \bullet \frac{1}{\pi t} \tag{10}$$

$$H\left[s(t)\right] = \frac{1}{\pi} \int_{-\infty}^{\infty} \frac{s(t)}{t-\tau} dt \tag{11}$$

where • is the convolution operator in (10) and H [$s(t)$] is an analytical part of the raw signal $s(t)$. Then, the fast Fourier transformation FFT is applied to the envelope signal *abs* (H [$s(t)$]) to extract fault characteristics from the amplitudes at the fault frequencies. After complete detection, the developed program automatically captures the faults frequency and corresponding amplitudes. Finally, the frequency features vector consists of fifteen elements representing the amplitudes at multiples of bearing fault frequencies (i.e., (1:5) ×BPFI, (1:5) ×BPFO and (1:5) ×BSF, respectively).

3. Experimental Work

In order to evaluate the proposed model, a bearing testbed was used. As shown in Fig .5, it consists of the following parts: electrical motor, coupling, a motion shaft, load, experimental bearing, and sensor. The self–aligning ball bearings (Bearing Number 1205) are employed as experimental bearing with different defect severity levels. Geometric parameters and calculated fault frequencies of the bearing are listed in Table 1. Artificial defects in the forms of spot and fine slit are created in bearing components (i.e., inner race, outer race, and ball) by two different types of electrical discharge machines (EDM) and measured by a microscope. Therefore, wire-cut EDM and drilled EDM are used for generated fine slit and spot faults, the samples of healthy and faulty bearing conditions are shown in Fig.6. The experimental work was done at the labs of the University of Basrah. The experimental bearing was applied to the non-drive end, and the accelerometer was attached in the horizontal direction with a sampling frequency equal to 48000 Hz. In this work, the data sets were recorded from 20 bearings and can be classified into five different conditions: normal, inner race faults, outer race faults, ball faults and combined faults During the experiment, three data sets were collected for three different speeds (i.e., 1200, 1500, and 1800 rpm). The time duration of each data is 100 seconds, and a segmentation process is applied with 5 seconds for a segment. Therefore, the segmentation process separates all the data sets into 20 samples each. Thus, the created fault dataset used for the experiments for each speed contains a total of 400 samples (20 normal samples + 5 inner fault severities × 20 samples + 6 outer fault severities ×20 samples + 6 ball fault severities ×20 samples + 2 combined fault severities ×20).

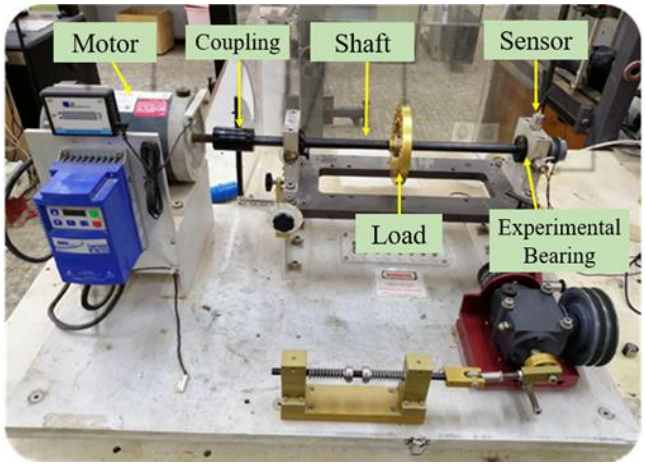

Fig .5 Test rig structures

Table 1. Bearing specification

Paramter	Value
Inner Diameter	25 mm
Outside Diameter	52 mm
Ball Diameter	7 mm
Width	15 mm
BPFI	7.11×Shaft Frequncy
BPFO	4.9×Shaft Frequncy
BSF	2.57×Shaft Frequncy
FTF	0.41×Shaft Frequncy

After all data sets are prepared, the feature vector is generated for each sample in the dataset. In MATLAB software, all the pre-processing steps and envelope analysis were done and we finally got three datasets with dimensions (400*15), each collected at a specific speed and can be employed in the future machine learning work. The details of the self–aligning ball bearing dataset with created faults are given in Table 2.

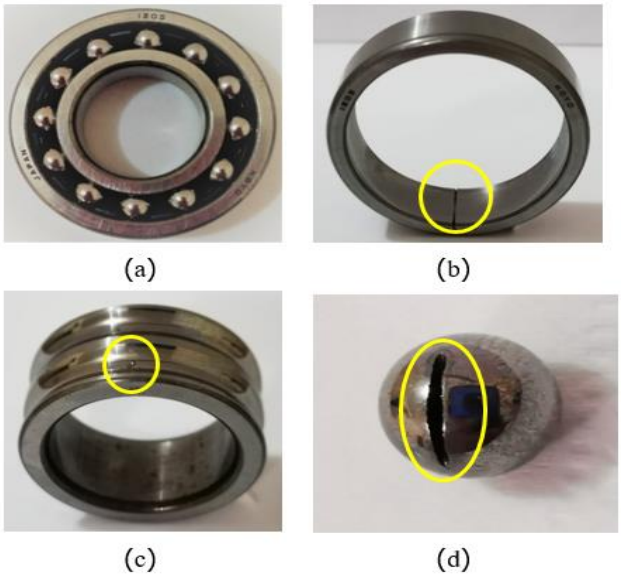

Fig. 6 Bearing conditions (a) healthy (b) outer race defect (c) inner race defect (d) ball defect

Table 2. Bearings and dataset specifications

Fault Type	Fault Size (mm)	Training Samples (1200 rpm)	Testing Samples (1500 rpm)	Testing Samples (1800 rpm)
Normal	none	20	20	20
Inner	0.4	20	20	20
	0.6	20	20	20
	0.7	20	20	20
	0.73	20	20	20
	0.98	20	20	20
Outer	0.39	20	20	20
	0.642	20	20	20
	0.86	20	20	20
	0.9	20	20	20
	1.047	20	20	20
	1.27	20	20	20
Ball	0.355	20	20	20
	0.4	20	20	20
	0.625	20	20	20
	0.75	20	20	20
	0.85	20	20	20
	1.12	20	20	20
Combined	Inner = 0.4 Outer =0.642 Ball =0.355	20	20	20
	Inner = 0.6 Outer =0.642 Ball =0.75	20	20	20

4. Experimental Results and Analysis

A bearing dataset with artificial faults was used to verify the effectiveness and feasibility of the proposed faults detection. Moreover, firstly the overall detection performance of the presented technique is tested based on the smallest fault sizes in datasets. In other words, checking the diagnosis ability diagnosis at an early stage of fault growth because the fault at this stage has low amplitude and short duration compared with surrounding noises leads to difficulty capturing reliable fault information and getting effective detection. In addition, after verifying from the diagnosis performance at the smallest faults can be applying this technique into other faulty bearings and different rotating speed. Also, this work employed the same validation procedure presented in [16,17], but they used data sets from other papers not collected in their works. In practice, the verification is done based on the following cases in the Table 3.

Table 3. Verification bearings specifications

Bearing Condition	Fault Size (mm)	Speed (RPM)	Fault Characteristic Frequency (Hz)
Normal	none	1200	none
Inner	0.4	1200	142.2
Outer	0.39	1200	97.8
Ball	0.355	1200	51.4
Combined	Inner = 0.4 Outer =0.642 Ball =0.355	1200	All of components

4.1. *Bearing Normal Vibration Signal Analysis*

The pre-filtering and diagnosis results of normal condition bearing are shown in Fig 7. The following figure is divided into sub-figures and described as follows. The raw signal was collected from the accelerometer sensor, the residual signal after removing the deterministic parts by the AR model, spectral kurtosis for selecting the best frequency band based on the maximum value, the envelope signal after applying the Hilbert transform and finally, the envelope spectrum and fault frequency features selection.

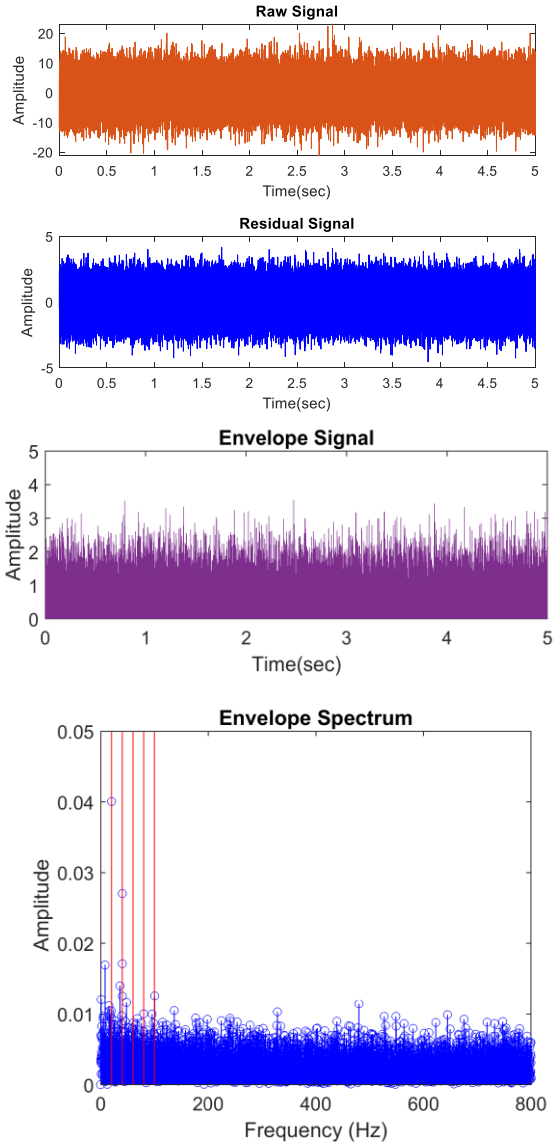

Fig.7 Pre-processing and envelope analysis results of normal condition.

As seen in figure 7, the raw signal of the normal condition has a small range between peaks value and after deleting the discrete part, the residual signal becomes smoother compared to the original signal. In addition, the SK value distribution appeared with two maximum peaks, but the developed program followed the exact maximum value and filtered the signal based on it. Also, the envelope spectrum doesn't detect any fault frequency but shows a small amplitude value at a rotating frequency (20 Hz) and can analyze as misalignment and this can prove that the proposed technique cannot detect the roller bearing problems only.

4.2. Inner Race Fault Vibration Signal Analysis

The pre-processing results and envelope analysis are illustrated in Fig .8, which includes the original vibration signal, residual signal and analyzed envelope.

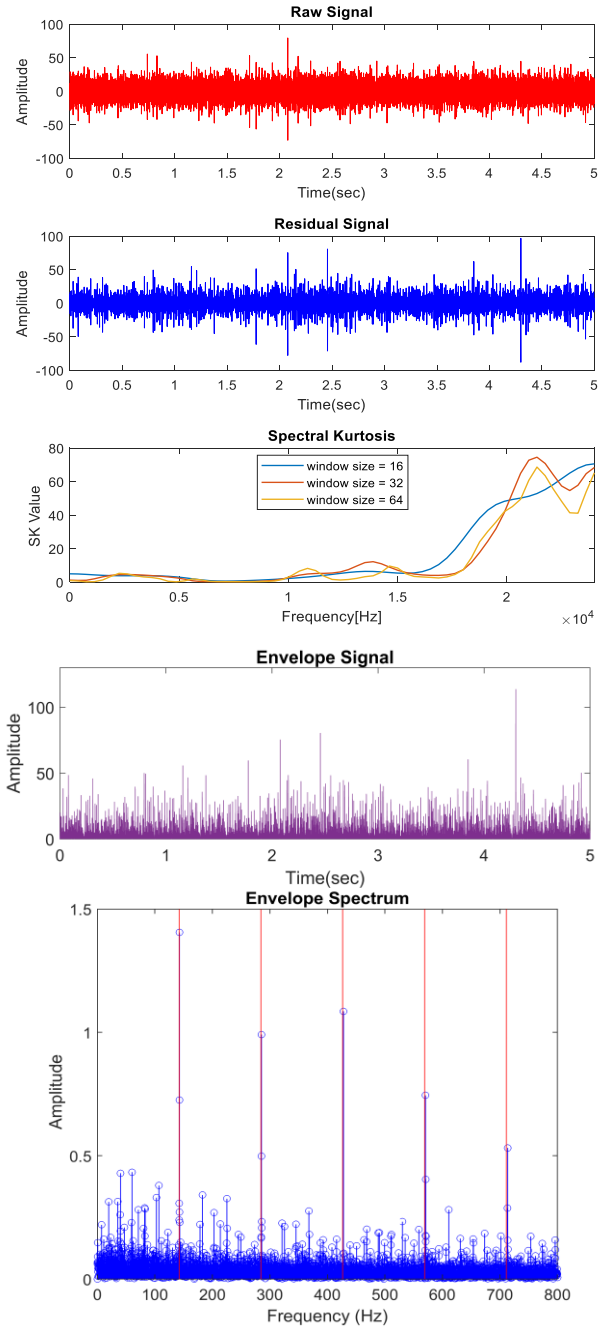

Fig.8 Pre-processing and envelope analysis results of inner race fault

As shown in figure 8, the raw signal has observable periodical peaks due to the fault in the inner race and can clearly distinguish after removing the discrete vibration noises. Also, the SK obtained the exact frequency band and can be seeing that through the envelope analysis results. From the spectrum can observe pure peaks at BPFI (142.2 Hz) and its harmonics. In addition, it can be seen that 1xBPFI has the largest peak, making fault detection proper for future fault classification.

4.3. Outer Race Fault Vibration Signal Analysis

The proposed detection results based on the outer race fault are shown in Fig.9. In the experiment, the raw signal is collected from the fault mounted in the sensor direction for getting intensive fault information.

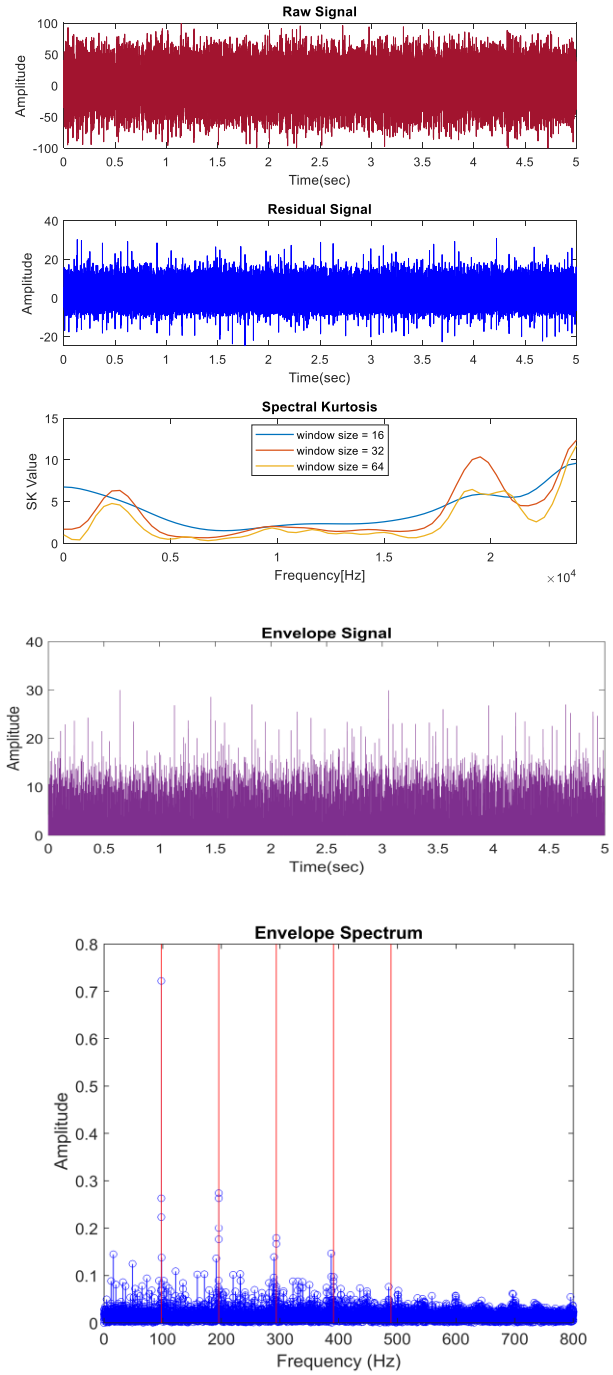

Fig.9 Pre-processing and envelope analysis results of outer race fault

From figure 9, it can be seeing the presented method achieved the aims of the work and effectively separated the outer fault signal from other vibration sources. Moreover, appeared gradually peaks at calculated BPFI (97.8Hz) and its harmonics in the envelope spectrum. Meanwhile, in every spectrum, should appear at least three harmonics to make sure there is a fault present.

4.4. Roller Fault Vibration Signal Analysis

In order to detect the roller fault, advanced detection techniques are required because the roller have rotating motion in multiple directions, slippage and clearance. Also, usually dominant roller faults at 2× BSF [18]. For this reason, verification from suggested method based on roller fault is illustrated in Fig.10.

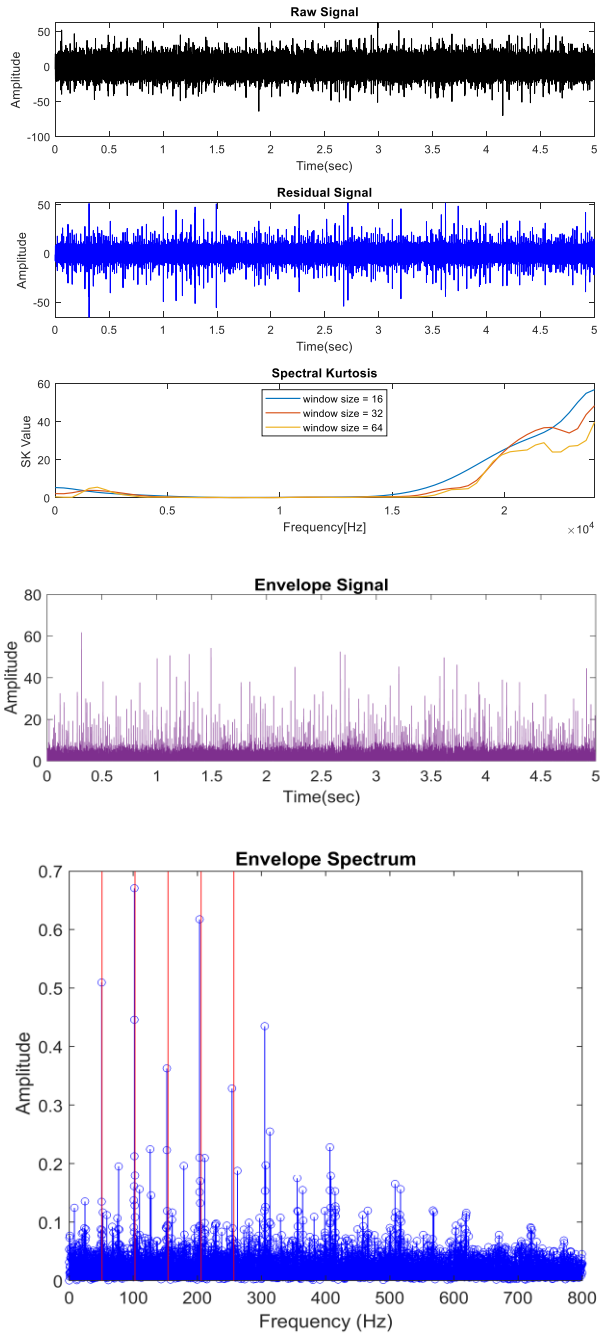

Fig.10 Pre-processing and envelope analysis results of roller fault

As is seen in figure 10, the residual signal has a lot of periodical spikes due to the roller fault striking the inner and outer races simultaneously. Also, it can be seen the first six harmonics of BSF (51.4 Hz) are outstanding in the spectrum and mostly in the roller fault cases the highest peak appeared at the second harmonic frequency.

4.5. Combined Fault Vibration Signal Analysis

In order to evaluate the presented method performance based on a combined fault so in the experiment employed three different faults in one roller bearing. Further, multiple vibration sources lead to increasing interference and overlapping between signals and become detection more difficult. The detection results based on the combined fault are shown in Fig.11.

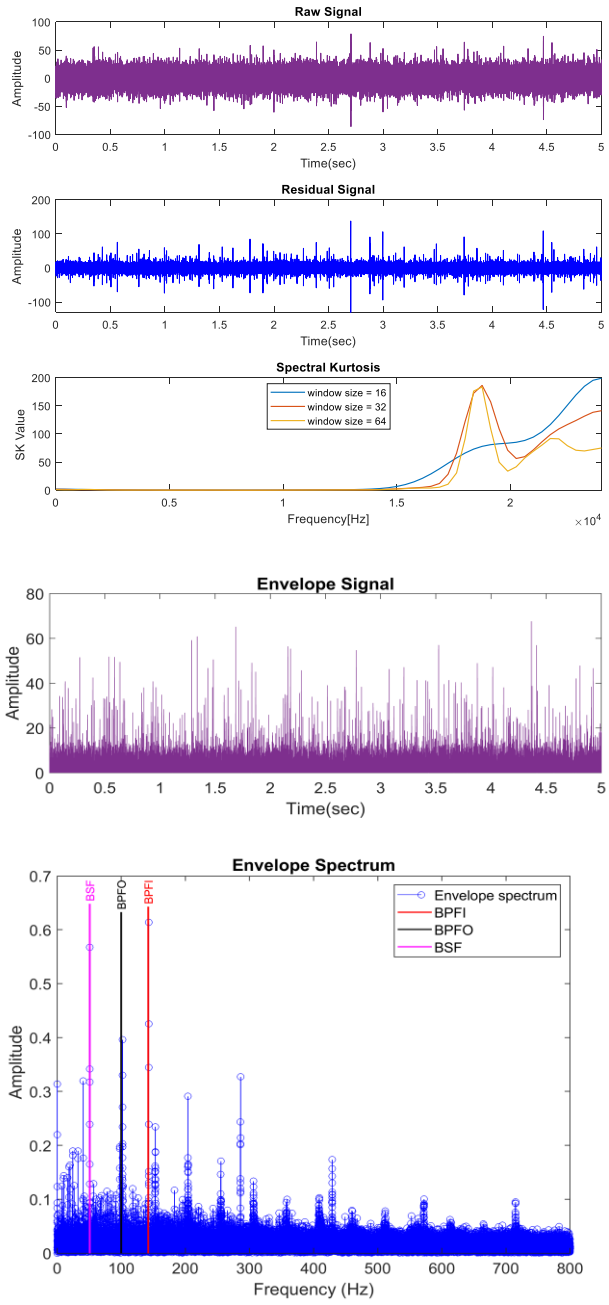

Fig.11 Pre-processing and envelope analysis results of combined fault

As seen in the above figure, all the fundamental fault frequencies and their harmonics are clearly obtained and can be fully recognized between peaks at resonance frequencies. The experimental results prove the proposed methods are effective for detecting roller bearing problems with different fault natures and under strong noise conditions. Furthermore, the final diagnosis results based on 1500 rpm and 1800 rpm for normal, inner race fault, outer race fault, ball fault and combined fault are presented in figures 12,13,14,15 and 16 respectively.

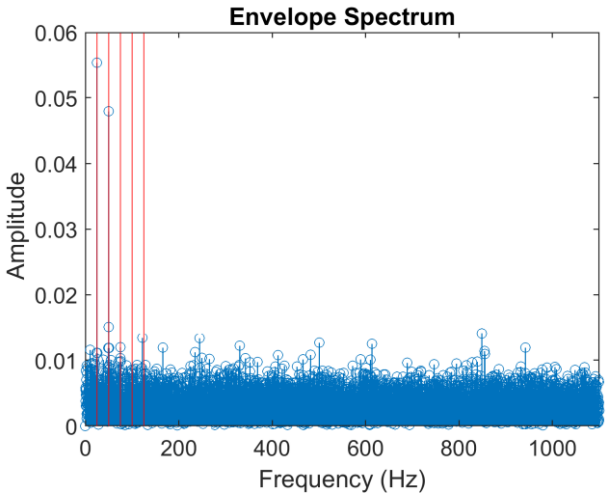

(a)

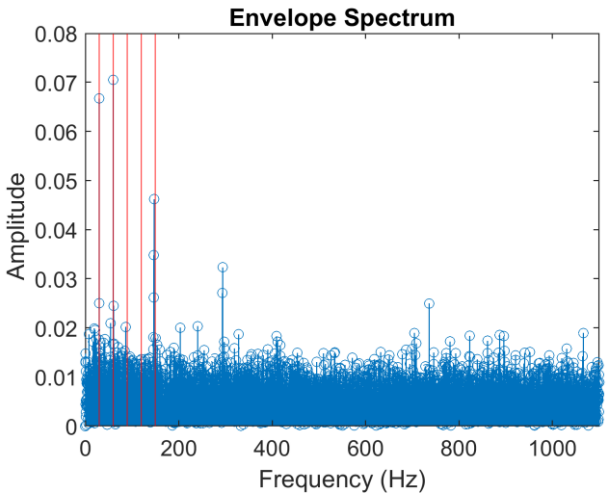

(b)

Fig.12 Diagnosis results of normal condition (a) at 1500 rpm (b) at 1800 rpm

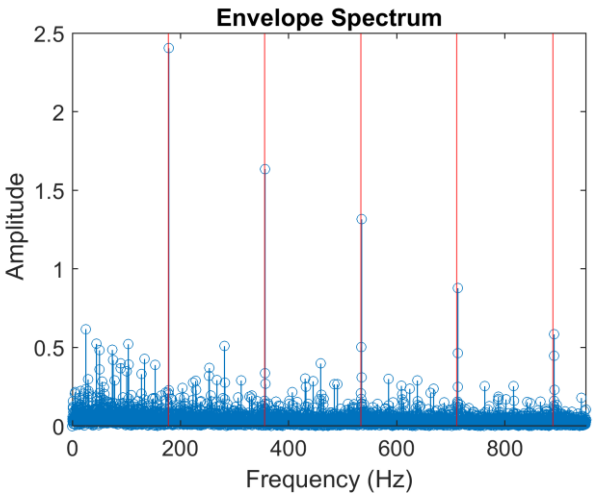

(a)

(b)

Fig.14 Diagnosis results of outer race fault (a) at 1500 rpm (b) at 1800 rpm

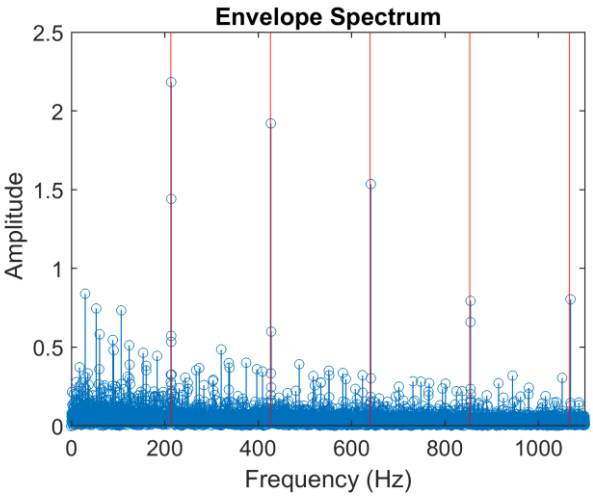

(b)

Fig.13 Diagnosis results of inner race fault (a) at 1500 rpm (b) at 1800 rpm

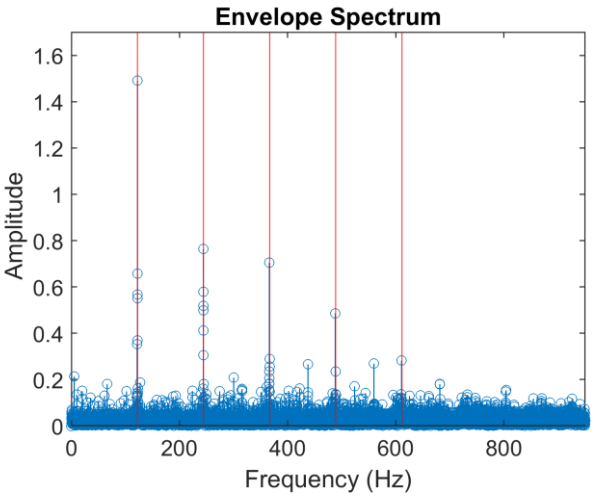

(a)

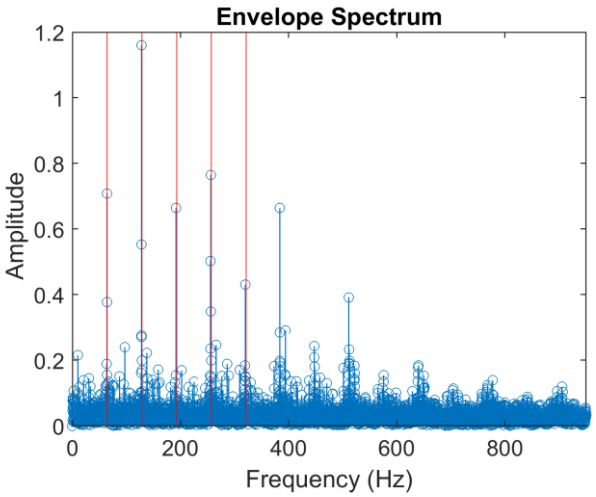

(a)

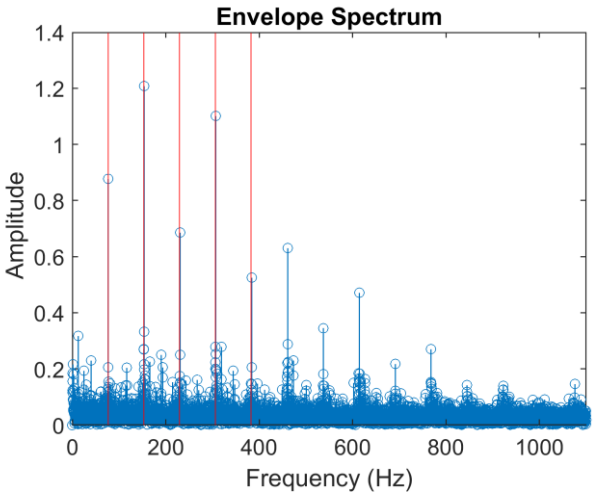

(b)

Fig.15 Diagnosis results of ball fault (a) at 1500 rpm (b) at 1800 rpm

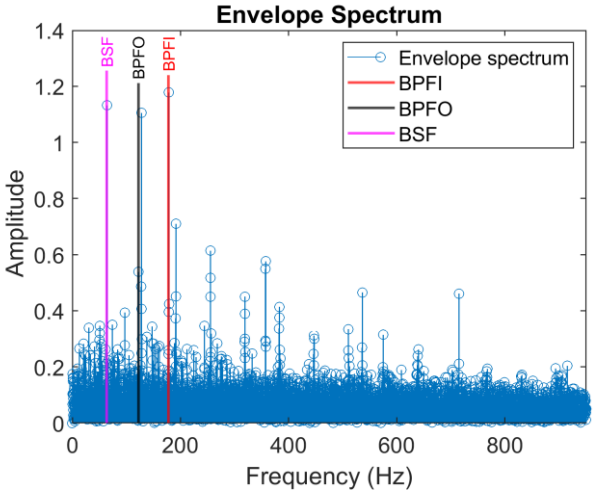

(a)

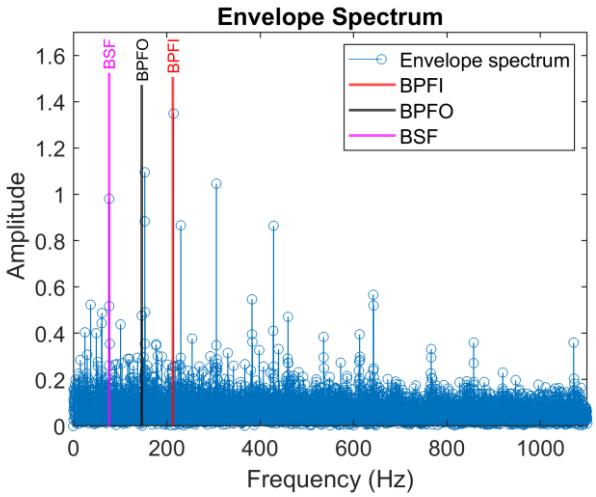

(b)

Fig.16 Diagnosis results of combined fault (a) at 1500 rpm (b) at 1800 rpm

The diagnosis results at 1500 rpm and 1800 rpm showed high detection accuracy for different roller bearing conditions. Finally, after totally complete the verification parts we applying the proposed method into other faulty bearing and getting frequency feature matrices based on three different speeds. The extracted features of the samples under study are summarized Table 4 ,5 and 6 for motor speed 1200 rpm, 1500 rpm and 1800 rpm respectively.

Table 4. Extracted features of samples at 1200 rpm

Peaks at Fundamental Fault Frequencies					
Frequency (Hz)	Normal Condition	Inner Fault	Outer Fault	Ball Fault	Combined Fault
1*BPFI	0.0084	1.4058	0.0338	0.0373	0.5603
2*BPFI	0.0085	0.991	0.0361	0.0348	0.3029
3*BPFI	0.0097	1.0851	0.0339	0.0317	0.1895
4*BPFI	0.0086	0.7451	0.0238	0.0518	0.1934
5*BPFI	0.0095	0.5318	0.0208	0.0565	0.1855
1*BPFO	0.0136	0.1169	0.7423	0.0672	0.5375
2*BPFO	0.01	0.08	0.3395	0.0888	0.5369
3*BPFO	0.0083	0.0897	0.2616	0.0557	0.3029
4*BPFO	0.0074	0.1596	0.1439	0.0644	0.1637
5*BPFO	0.0082	0.188	0.0671	0.043	0.1199
1*BSF	0.0078	0.1238	0.0255	0.5095	0.6856
2*BSF	0.0074	0.3311	0.0352	0.6726	0.5375
3*BSF	0.0084	0.1294	0.0238	0.3611	0.5603
4*BSF	0.0079	0.1245	0.0418	0.6156	0.5369
5*BSF	0.0077	0.0808	0.026	0.3283	0.3294

Table 5. Extracted features of samples at 1500 rpm

Peaks at Fundamental Fault Frequencies					
Frequency (Hz)	Normal Condition	Inner Fault	Outer Fault	Ball Fault	Combined Fault
1*BPFI	0.00623	2.40464	0.06580	0.04955	1.17852
2*BPFI	0.006185	1.63470	0.05546	0.04661	0.576652
3*BPFI	0.005981	1.31606	0.01327	0.04829	0.464748
4*BPFI	0.004533	0.87791	0.01984	0.04355	0.460938
5*BPFI	0.007822	0.58414	0.03512	0.06736	0.20422
1*BPFO	0.008925	0.10730	1.49837	0.07839	1.105681
2*BPFO	0.017164	0.09189	0.76223	0.02751	0.614145
3*BPFO	0.008399	0.07291	0.70137	0.05630	0.576652
4*BPFO	0.007706	0.07909	0.48665	0.03388	0.175167
5*BPFO	0.006384	0.0804	0.13095	0.022196	0.189319
1*BSF	0.004979	0.0553	0.03460	0.70798	1.131905
2*BSF	0.00586	0.0489	0.03025	1.16397	1.105681
3*BSF	0.005829	0.04519	0.01134	0.66528	0.709785
4*BSF	0.006511	0.15465	0.02941	0.76029	0.614145
5*BSF	0.007293	0.06795	0.05141	0.43132	0.449958

Table 6. Extracted features of samples at 1800 rpm

Peaks at Fundamental Fault Frequencies					
Frequency (Hz)	Normal Condition	Inner Fault	Outer Fault	Ball Fault	Combined Fault
1*BPFI	0.009488	2.18293	0.06586	0.03990	1.348438
2*BPFI	0.007887	1.92063	0.04335	0.04094	0.863895
3*BPFI	0.007205	1.53455	0.03741	0.03964	0.566529
4*BPFI	0.01153	0.79458	0.03950	0.03981	0.359089
5*BPFI	0.017914	0.80207	0.05802	0.05066	0.35934
1*BPFO	0.043852	0.14770	2.13007	0.05345	1.095097
2*BPFO	0.030677	0.08740	1.82612	0.05346	1.045079
3*BPFO	0.011986	0.10499	1.07686	0.04243	0.863895
4*BPFO	0.012077	0.11377	0.21527	0.03781	0.272207
5*BPFO	0.009447	0.04955	0.20267	0.02425	0.174474
1*BSF	0.01417	0.09857	0.03566	0.87760	0.98074
2*BSF	0.010709	0.19592	0.03345	1.20812	1.095097
3*BSF	0.013297	0.12844	0.02239	0.68553	0.865319
4*BSF	0.012221	0.07243	0.02867	1.100669	1.045079
5*BSF	0.011658	0.08219	0.03767	0.52477	0.546772

5. Conclusions

This paper proposed a more general and effective faults feature extraction technique applicable to rolling element bearings. The following conclusions could be drawn from the work:

1. The features extracted represented the acceleration peaks at fundamental fault frequencies of roller bearing.
2. The proposed method involves pre-processing and envelope analysis methods. In the pre-processing stage, the AR model is employed for separating the fault signals from other deterministic components.
3. The best center frequency is selected based on the maximum SK value with narrow bandwidth to eliminate as much as possible the other vibration sources from passing to the next analysis process.
4. The filtered signal is analyzed by using the envelope approach to distinguish between bearing faults characteristics and make the frequency features clearer and easily extracted.
5. A bearing dataset containing different levels of fault severities and health conditions was used to validate the proposed method, especially the bearing in the early stage of fault growth. Also, each bearing condition was collected at three different rotating speeds.
6. The diagnosis results showed the developed method effectively extracts the features at calculated resonance bearing frequencies and proves the significance of the enhancements in a pre-filtering stage in the overall detection performance.
7. Based on experimental findings, the future direction of work benefits from the developed method on faults diagnosis and classification at different speeds because the frequency features are independent of both speed variation and bearing type.

References

[1] J. Alsalaet, Q. T. Alhadithi and S. N. Abdulkareem, “Multi fault detection of the roller bearing using the wavelet transformand principal component analysis”, International Journal of Energy and Environment, vol.7, no.6 pp.519–528, 2016.

[2] A. A. Abdulrazzaq, “Diagnosis of Rotating Machines Faults Using Intelligent Methods”, M.S. thesis, College of Eng., Basrah Univ., Basrah, Iraq, 2019.

[3] A. A. Abdulrazzaq and J. K. Ali, “Surveys for artificial immune recognition system and comparison with artificial neural networks and support vector machines in intelligent fault diagnosis of rotating machines”, Int. J. Mech. Eng. Technol., vol. 10, no. 1, pp. 1686–1709,2019.

[4] D. Abboud, J. Antoni, S. Sieg-Zieba, and M. Eltabach, “Envelope analysis of rotating machine vibrations in variable speed conditions: A comprehensive treatment”, Mech. Syst. Signal Process., vol. 84, pp. 200–226, 2017.

[5] H. Q. Wang, W. Hou, G. Tang, H. F. Yuan, Q. L. Zhao, and X. Cao, “Fault detection enhancement in rolling element bearings via peak-based multiscale decomposition and envelope demodulation”, Math. Probl. Eng., vol. 2014, 2014.

[6] E. Bechhoefer, M. Kingsley and P. Menon, “Bearing envelope analysis window selection Using spectral kurtosis techniques”, 2011 IEEE Conference on Prognostics and Health Management, 2011.

[7] A. Amini, M. Entezami, and M. Papaelias, “Onboard detection of railway axle bearing defects using envelope analysis of high frequency acoustic emission signals”, Case Studies in Nondestructive Testing and Evaluation, Vol.6, 2016

[8] P. Xu, A. Ghasemloonia, and Q. Sun, “Automatic band selection algorithm for envelope analysis,” Proc. Inst. Mech. Eng. Part C J. Mech. Eng. Sci., vol. 233, no. 5, pp. 1641–1654, 2019.

[9] L. Jia, L. Jiang, and Y. Wen, “A Two-Stage Method for Weak Feature Extraction of Rolling Bearing Combining Cyclic Wiener Filter with Improved Enhanced Envelope Spectrum”, Machines, vol. 10, no. 10, p. 863, 2022.

[10] W. A. Smith and R. B. Randall, “Rolling element bearing diagnostics using the Case Western Reserve University data: A benchmark study”, Mech. Syst. Signal Process., vol. 64–65, pp. 100–131, 2015.
[11] W. Caesarendra, “Vibration and acoustic emission-based condition monitoring and”, Ph.D. dissertation, Dept. of Mechanical, Materials and Mechatronic Eng., University of Wollongong, Australia, 2015.
[12] R. B. Randall, Vibration-based condition monitoring: Industrial, aerospace and automotive applications, London: John Wiley, 2010, ISBN: 978-0-470-74785-8.
[13] S. Kim, D. An, and J. H. Choi, “Diagnostics 101: A tutorial for fault diagnostics of rolling element bearing using envelope analysis in MATLAB”, Appl. Sci., vol. 10, no. 20, pp. 1–23, 2020.
[14] R. B. Randall and J. Antoni, “Rolling element bearing diagnostics-A tutorial”, Mech. Syst. Signal Process., vol. 25, no. 2, pp. 485–520, 2011.
[15] M. Sohaib, C. H. Kim, and J. M. Kim, “A hybrid feature model and deep-learning-based bearing fault diagnosis”, Sensors (Switzerland), vol. 17, no. 12, 2017.
[16] W. A. Smith and R. B. Randall, “Rolling element bearing diagnostics using the Case Western Reserve University data: A benchmark study,” Mech. Syst. Signal Process., vol. 64–65, pp. 100–131, 2015.
[17] W. Li, M. Qiu, Z. Zhu, B. Wu, and G. Zhou, “Bearing fault diagnosis based on spectrum images of vibration signals,” Meas. Sci. Technol., vol. 27, no. 3, 2016.
[18] W. Li, M. Qiu, Z. Zhu, F. Jiang, and G. Zhou, “Fault diagnosis of rolling element bearings with a spectrum searching method”, Meas. Sci. Technol., vol. 28, no. 9, 2017.